Chapter V: Temperature dependent exchange bias, training effect and memory effect of core-shell $CoCr_2O_4$ particles.

5.1 Introduction

Reduction in grain size has led numerous technological applications of magnetic nanoparticles in magnetic recording media, ferrofluids, spin valves, magnetic tunnel junctions, magnetic refrigeration etc. [Tsang et al. (1994); Kools et al. (1996); Guo et al. (2009)]. However, there the limitation is the instability of ferro/ferri-magnetic behavior of the nanoparticles because of their thermal fluctuations. To enhance the thermal stability of magnetic materials, composites with high anisotropy have been synthesized. New attempt is made to make nanoparticle composites particularly of core shell structure where high-anisotropy and exchange bias improve the thermal stability [Meiklejohn et al. (1957); Nogues et al. (2005)]. In case of nanoparticles, the exchange bias (EB) effect could be established by a system which contains two kinds of exchange coupled spins such as frozen spins that cannot be reversed and the other rotatable spins that can be reversed by applyng field [Zhu et al. (2015)]. Core-shell structure of nanoparticles is an example, where a collinear ferrimagnetic spins surrounded by a non-collinear antiferromagnetic spins are expected to show exchange bias phenomena as generally reported in the interface of ferromagnetic-antiferromagnetic (FM-AFM) layers [Nogues et al. (1999), Berkowithz et al. (1999)]. Baaziz et al., reported the high exchange bias (H_E=4.1 kOe) between FIM and the AFM components and high coercive field (15 kOe) at 5 K in core shell nanoparticles where core and shell are of $Fe_{3-\delta}O_4$ and CoO respectively. Hence, the core-shell structures represent promising systems to enhance the

magnetocrystaline anisotropy at the nanoscale [Baaziz et al. (2013)]. Although, exchange bias in spin glass [Ali et al. (2007)] and in core-shell nanoparticles [Mumtaz et al.(2007), Maaz et al. (2009)] have been reported, we have examined here the exchange bias effect in core-shell $CoCr_2O_4$ nanoparticles which exhibits a long range ferrimagnetic core and spin glass shell. Another interesting phenomenon known as "training effect" which is generally observed in FM/AF systems when the sample is kept under continuous filed loops. In training effect, the exchange bias is found to vary with the number of hysteresis loops [Keller et al. (2002); Ali et al. (2003)]. Training effect combining with exchange bias phenomena are important features to be studied in core shell structure. $CoCr_2O_4$ of 50 nm particles with core shell structure where core exhibits long range ferrimagnetic order and disordered spins existing in the shell shows spin glass (SG) behavior [Jagadish et al. (2016)]. We examine the exchange bias, training effect and temperature dependent memory effect in $CoCr_2O_4$ of 50 nm particles having core-shell structure.

We have discussed the microstructure of 50 nm $CoCr_2O_4$ nanoparticles in section 5.2.1.Section 5.2.2 discusses the magnetic properties like exchange bias, training effect and memory effect. The results are summarized in section 5.3.

5.2. Results

5.2.1. Microstructural analysis

$CoCr_2O_4$ of 50 nm particles synthesized through conventional co-precipitation technique demonstrate pure, cubic phase of Fd-3m space group. The field emission scanning electron micrograph of $CoCr_2O_4$ is shown in Fig. 5.2.1.

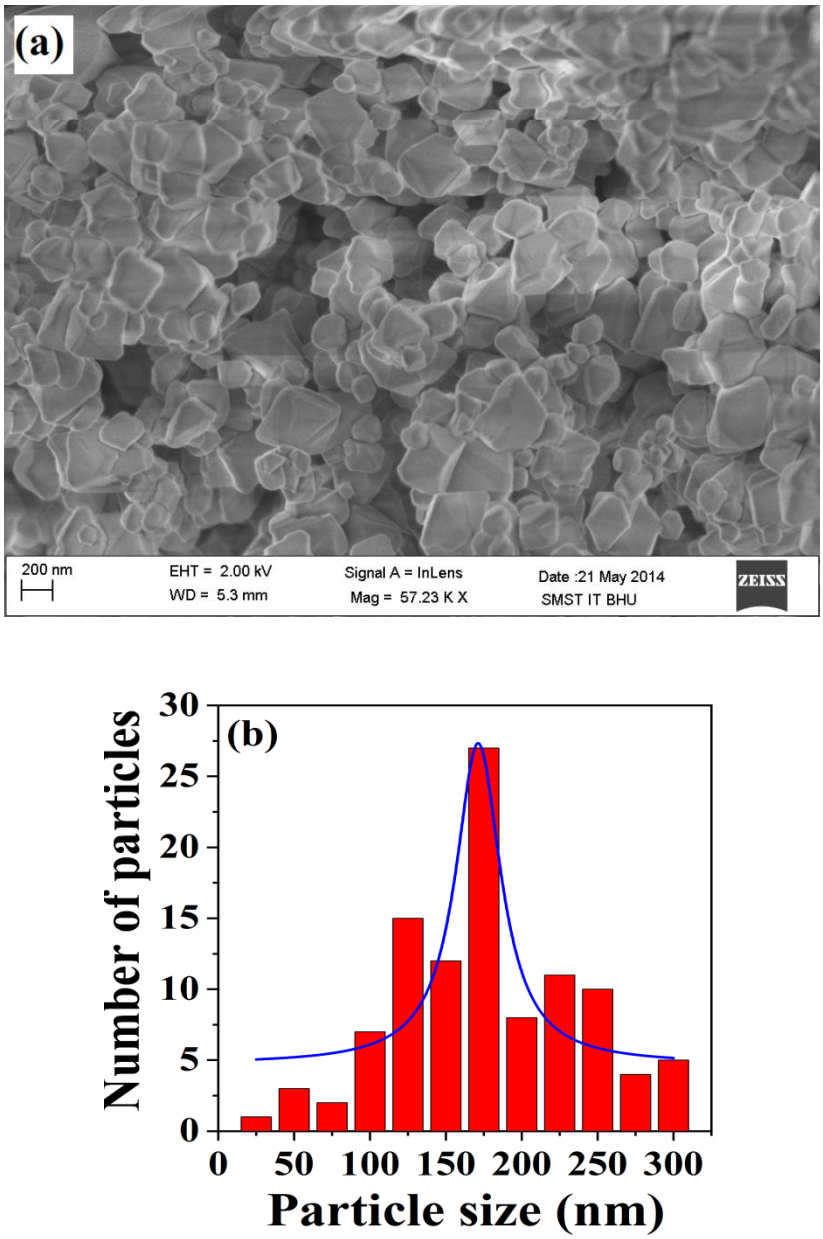

Fig. 5.2.1 (a) Field emission scanning electron micrograph of $CoCr_2O_4$ and **(b)** particle size histogram.

The particles are mostly agglomerated and the mean particle size is found to be in the range of 160-170 nm. Extended X-ray Absorption Fine Structure Spectroscopy (EXAFS) studies on Co and Cr K-edges analyzed using ATHENA and ARTEMIS of FEFF 8.0 code confirm that Co ions prefer tetrahedral (A) site and Cr ions prefer octahedral (B) site

without showing any change in their cation distribution even after reducing the size to 50 nm [Jagadish et al. (2016)]. The temperature dependent magnetization measured under ZFC and FC conditions at 10 kOe field show paramagnetic to long range ferrimagnetic transition at 100 K and a short range, commensurate spiral ordering at spin-spiral transition 26 K (Fig. 4.2.6 (b)**)**. From ac susceptibility measurements done at frequencies 3, 31, 230, 966 Hz under applied field of 3 Oe, we reveal that while the real part of a.c susceptibility (χ') peak show no dispersion behavior, the imaginary part (χ'') splits into two prominent peaks with a shifting towards higher temperature with increasing frequency [Fig. 4.2.7 (b)]. The two peak behavior indicates that 50 nm particles here show core shell structure. The observation is well supported by Godsell *et al.* [Godsell et al. (2011)]. We further performed hysteresis measurements at various temperatures to support core shell structure of these nanoparticles and reported elsewhere [Jagadish et al. (2016)]. The frequency dependent T_B fitted with an empirical relation [$\Phi=\frac{\Delta T_B}{T_B \Delta \log_{10} \omega}$] show the spin glass nature [Mydosh et al. (1993)] which is further confirmed from the memory effect experiment. Complete analysis of structure, microstructure from XRD, EXAFS and magnetic properties using magnetic measurements have been discussed in chapter IV. It is confirmed that $CoCr_2O_4$ nanoparticles exhibit a ferrimagnetic core surrounded by a thin shell of spin glass. Here we further examine the exchange bias effect, training effect, temperature dependent memory effect and their inter-dependence due to the core-shell nature of these nanoparticles.

5.2.2 Magnetic Properties

5.2.2.1 Exchange bias effect

Fig. 5.2.2 depicts the hysteresis loops measured at various temperatures under 10 kOe cooling field. The hysteresis loops are not saturated up to ±70 kOe irrespective of measuring temperatures.

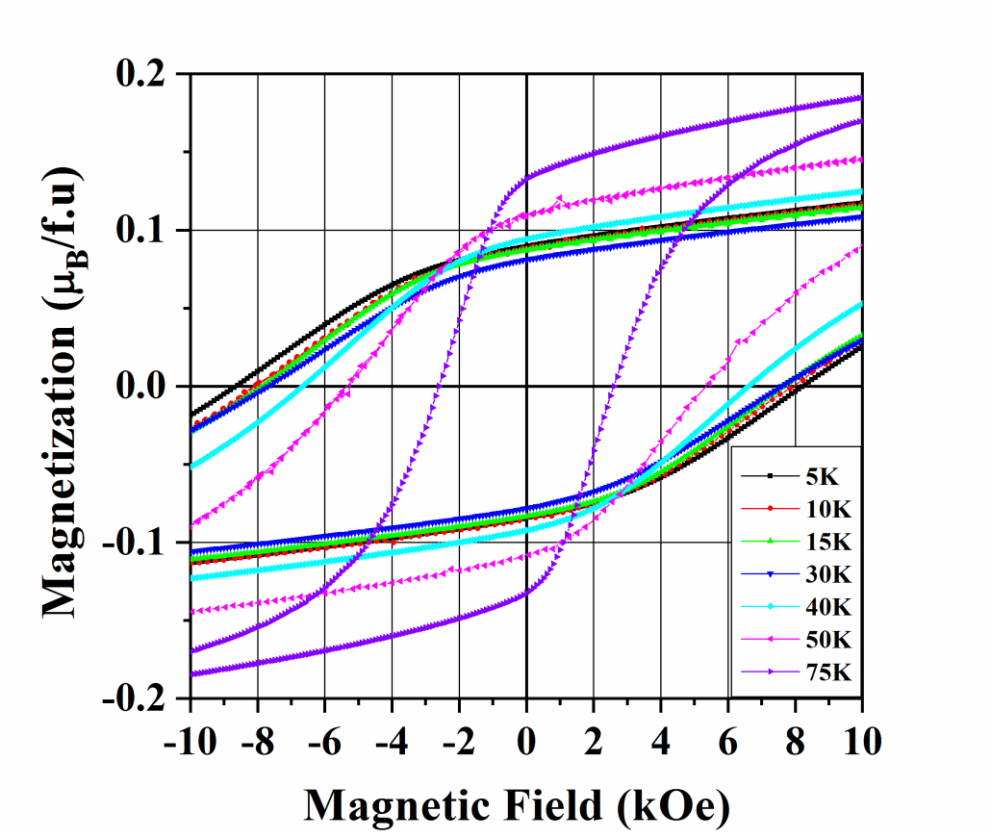

Fig.5.2.2 Hysteresis loops of $CoCr_2O_4$ measured under field cool condition of 10 kOe field at various temperatures.

The magnetization increases readily at low fields and then linearly increases up to 70 kOe. The non-saturation of magnetization results from the large contribution of disordered spins at the surface. With decrease in temperature from 75 K to 5 K, the loop is found to shift towards negative H-axis. The magnitude of exchange field, H_{EB} is

calculated using $-\frac{(H_{C+}+H_{C-})}{2}$ and the effective coercive field is calculated using $H_c^{eff} = \frac{(H_{C+}-H_{C-})}{2}$, where H_{C+} and H_{C-} are positive and negative coercive fields respectively. While a small exchage bias of 0.5 Oe and effective coercive field of 5 kOe is observed at 75 K, the exchange bias is increased to 205 Oe and the effective coercive field increases to 8.5 kOe at 5 K. The high exchange bias at low temperature (below 10 K) could be explained using cluster dynamics. Below 10 K, the exchange interaction dominates the thermal fluctuations hence the magnetic ordering of these clusters grow and can't reverse their magnetization easily. The increase in internal effective field generated by clusters along with increase in magnetization is responsible for the observed exchange bias in FC condition. The vertical magnetization shift (M_{EB}) is calculated using $M_{EB} = -\frac{(M_{R+}+M_{R-})}{2}$ where M_{R+} and M_{R-} are the positive and negative remenant magnetization. The vertical magnetization shift of $8.5x10^{-3}\mu_B$/f.u observed at 5 K could be due to the presence of net uncompensated spins remaining frozen along the drection of cooling-field. Comparing the reported H_{EB} (~5 Oe) and M_{EB} (~$2.5x10^{-4}\mu_B$/f.u) observed at 5 K by Padam *et al.* in bulk $CoCr_2O_4$, H_{EB} is found to be two orders of magnitude and M_{EB} is one order of magnitude higher in these nanoparticles [Padam et al. (2014)]. This is indicative of the development of unidirectional anisotropy in the non-collinear spiral ordering. In contrast to earlier reports by Padam et al., where H_{EB} is found to increase steeply below lock-in temperature (~10 K) with decrease in temperature due to change in incommensurate to commensurate spin-spiral, we observe an unusual high exchange bias which starts at 50 K [Padam et al. (2014)]. The EB in cobalt chromite nanoparticles originates due to interactions between ferrimagnetically aligned core and disordered frozen surface spins at the shell. Montey Carlo study of the exchange bias in nanoparticles consisting of a

ferromagnetic (FM) core and an antiferromagnetic (AFM) shell demonstrates that the exchange interaction at the interface having a strong anisotropy results in an exchange bias field (H_{EB}) and a strong coercive field (H_c) [Visalkaki et al. (2008)]. The schematic diagram of core-shell structure having ferrimagnetic core and shell of spin-glass is shown in Fig. 5.2.3(a). Below 50 K, the core/shell interactions develop due to the blocked surface spins along their anisotropy axes. The exchange bias increases with decrease in temperature due to increase in core shell interactions as the thermal fluctualtions decreases with decrease in temperature. Above 50 K, the core/shell interactions decrease due to de-blocking of surface spins and hence EB vanishes. Much higher EB than the bulk phase is attributed to commensurate spin-spiral transition observed in these nanoparticles which we have found using diffused neutron scattering as discussed in chapter IV. Thus, origin of exchange bias is not only due to interface bewteen collinear and non-collinear spins, but also contributed by the spin spiral ordering observed below 26 K. Similar EB effects are also reported by Muroi *et al.* for the nanosized $La_{0.7}Ca_{0.3}MnO_3$ with a FM core and a spin glass shell [Muroi et al. (1999)]. In order to study the field dependent EB effect, M-H loops are measured upto ±70 kOe and ±50 kOe under FC condition at 10 kOe field and are depicted in Fig. 5.2.3(b).

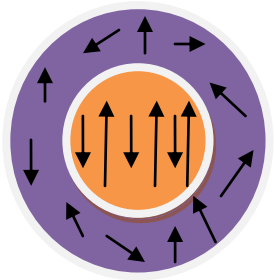

Fig.5.2.3(a) Schematic representation of core-shell nanoparticles having core ferrimagnetic and shell of spin-glass.

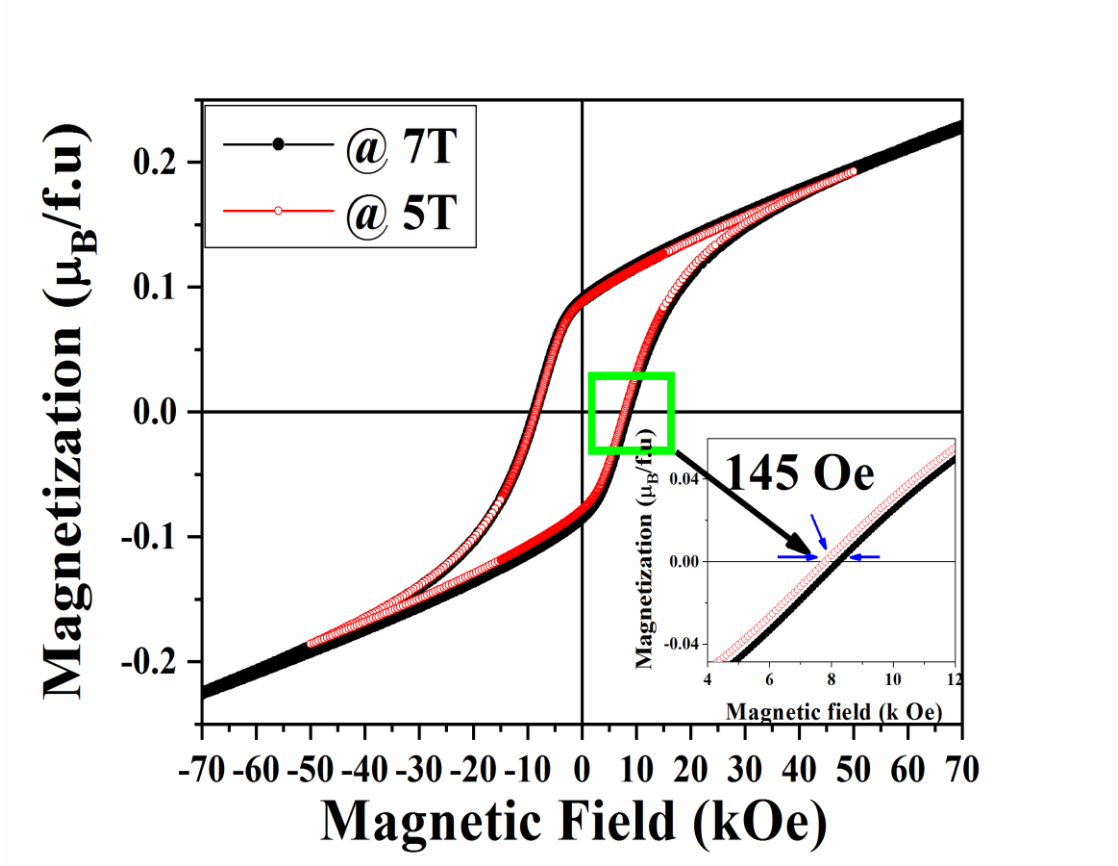

Fig. 5.2.3(b) The difference in exchange field observed when loop is measured up to 50 kOe and 70 kOe at 5 K**.**

Higher exchange bias of 145 Oe is observed when the M-H loop is measured at 5 K upto 50 kOe than measured upto 70 kOe. The less EB at higher applied field (70 kOe) has been attributed to the high field effects on the surface (shell) spins. At higher fields, the shell spins align along the field direction and hence weakens the core-shell interface interactions. As a result, we observe a reduction in the exchange bias. Similar observations have been reported by Maaz *et al* in $CoFe_2O_4$ nanoparticles having core shell structure [Maaz et al. (2009)]. In order to understand such complex phenomena like exchange bias, we have studied the training effect.

5.2.2.2. Training effect

Training effect is studied by measuring exchage bias under FC condition after repeated nummber of hysteresis loops. The sample is cooled from 300 K to 5 K in presence of 10 kOe field and consecutive hysteresis loops are measured for 7 times. Fig. 5.2.4. depicts the continuous hysteresis loops with index n=1 to 7. The gradual decrease in H_{EB} with increasing loop cycle shown in Table 5.2.1 is a characteristic feature of training effect. The percentage of training effect TE (%) is defined as the relative decrease in H_{EB} with increasing number of cycles.

$$TE\ (\%) = \left(1 - \frac{H_{EB}^{1} - H_{EB}^{n}}{H_{EB}^{1}}\right) \times 100(\%) \quad \text{---------- (5.1)}$$

Where H_{EB}^{n} is the exchange bias field of the n^{th} cycle.

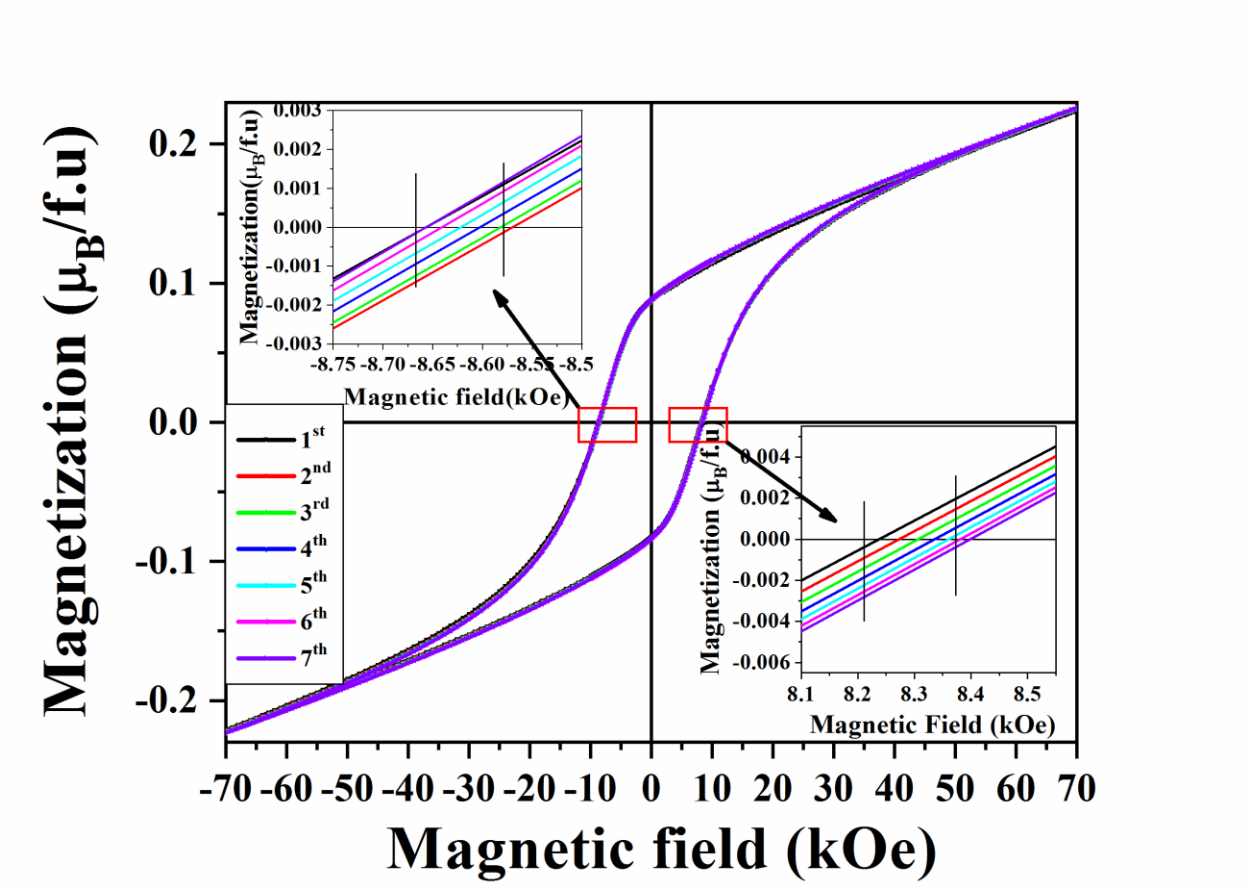

Fig. 5.2.4 Training effect observed in 7 loops. Changes in magnetic hysteresis loop from first to seventh cycle is shown in inset.

Table 5.2.1: Numeric values of exchange bias field (H_{EB}) and percentage of training effect during each cycle.

No. of loops (n)	$H_{EB}=(H_{C+}+H_{C-})/2$ (Oe)	% of TE
1	212.5	100
2	149.5	70.3
3	145	68.2
4	135	63.5
5	130	61.2
6	130	61.2
7	127.5	60

From Table 5.2.1, one may note that, with increase in number of loops, the percentage of training effect decreases and attains 60% after 7^{th} cycle. The percentage of decrease of H_{EB} between the first and second loop is 30% which is larger than the subsequent loops. This indicates that the magnetization relaxes much quickly from first loop to second loop than the consequtive loops. The percentage of training effect and M_{shift} has a similar decrease in tendency with number of cycles. Hence, the linear dependence of TE and M_{shift} are closely connected with decrease in fraction of pinned uncompensated spins upon field cycling [Zhu et al. (2015)]. Hence the training effect could be explained by pinned uncompensated spins at the interface. In this context, in order to understand the microscopic mechanism of training effect, the experimental data is fitted using two equations such as power law and Landau-Khalatnikov (LK) equation.

For number of loops (n) >1, the training effect is analyzed using power law as given below

$$H_E(n) - H_{E\infty} = \frac{k}{\sqrt{n}} \qquad \text{---------- (5.2)}$$

$H_{E\infty}$ is the EB field in the limit of an infinite number of loops and *k* is a system dependent constant. Inset of Fig. 5.2.5 shows the fitted experimental data in equation (5.2) with the estimated values of *k* and $H_{E\infty}$ are 135.9 and 68 Oe respectively. One may notice that after one cycle H_{EB} drops drastically followed be gradual decrease in H_{EB} with increase in loop cycle from n=2 to 7. Therefore, we expect that the phenomenological relaxation theory could provide proper description of training effect in our case. Hence, the phenomenological model proposed by Binek *et al.* is considered to explain the training effect in the framework of non-equilibrium thermodynamics based on relaxation theory

[Binek et al. (1999)]. The above model is a recursive sequence derived from Landau-Khalatnikov (LK) equation and is given below:

$H_E(n+1) - H_E(n) = - \gamma (H_E(n) - H_{E\infty})^3$ ---------- (5.3)

γ is the characteristic decay rate of the training behavior. Fig. 5.2.5 depicts the fitting of H_E vs. n using equation (5.3).

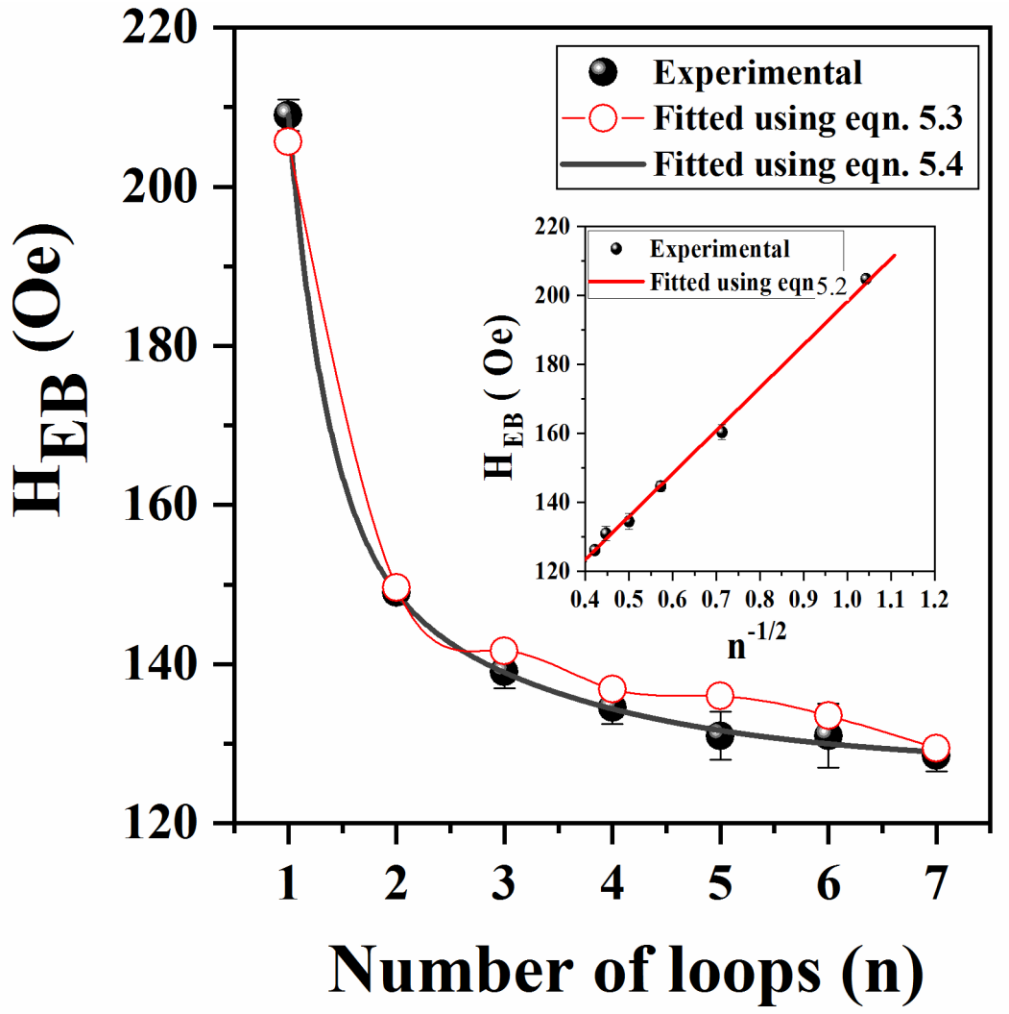

Fig. 5.2.5. Experimental exchange bias H_{EB} (solid circles) fitted using equation (5.3) (open circle) and equation (5.4) (line). Inset show fitting of experimental data using power law, (H_{EB}) Vs $n^{-1/2}$. The exchange-bias (H_{EB}) data is obtained at 5 K after field cooling under 10 kOe field.

The obtained values of ɣ and $H_{E\infty}$ are 10^{-5} Oe^{-2} and as 68 Oe respectively. A small value of ɣ observed from fitting signifies large deviation from the equilibrium steady state and corresponds to large training effect [Guo et al. (2010)]. This further indicates that such phenomenon is relevant for spin glass behavior. As a consequence, consecutive cycle of field reversal could not able to change the spins of spinglass state along the direction of cooling field. Because these spins fall in an another metastable configuration. Hence, the contribution of these spins to exchange coupling is reduced at the interface and the exchange bias field is decreased with loop cycle. One may notice a small deviation of experimental data at higher n values. This could be due to decrease in H_{EB} between the first and second loop is higher than the subsequent loops. It indicates that the magnetization relaxes much more quickly from the first loop to the second loop than in the higher loops. Hence, the presence of only one exponent in the expression could not describe the training effect completely. The H_{EB} dependence on cycle number involves two mechanisms which describe the difference in H_{EB} between first and second loop, the other describes the monotonic decrease in H_{EB} in higher loops. While the former mechanism could arise from the AFM symmetry, the later one is attributed to reconfiguration of AFM moments or domains during continuous magnetization cycle [Wang et al. (2015)]. The spin rearrangement takes place during each cycle modifies H_{EB}. Hence the following multiple exponent expression may fit with the experimental data exactly for all values of n.

$$H_E(n) - H_{E\infty} = A_f \exp(-n/P_f) + A_r \exp(-n/P_r) \text{ ---------- (5.4)}$$

Where, A_f and P_f are parameters related to change of frozen spins and A_r and P_r correspond to rotatable spin parameters of the magnetic frustration [Wang et al. (2015)].

Fig. 5.2.5 depicts the best fit of experimental data using equation (5.4) results to $H_{E\infty}$ = 127.3, A_f = 865 Oe, P_f =0.3542, A_r= 49 Oe and P_r=2.0647. The large difference between A_f and A_r and P_f and P_r indicates that the rotatable spins dominate over the frozen spins. Hence, the frozen/pinned spins are unstable during each magnetization reversal and hence H_E decreases. This feature corroborates with the spin glass behavior.

5.2.2.3. Memory effect

Memory effect in ZFC protocol demonstrates an intrinsic process of cooperative nature of spin-spin correlation having randomly frustrated interaction, which is usually noticed in the atomic SG system [Bisht et al. (2010)]. While core shows a long range ferrimagnetic behavior, the shell shows a spin glass type, we perform the memory effect experiment in ZFC protocol which is a finger print of spin-glass behavior. In order to study the memory effect experiment, we followed the protocol proposed by T. Jonsson *et al.*[Jonsson et al. (1999)] and Sun *et al.* [Sun et al. (2003)]. The sample is cooled in zero magnetic field down to 2 K from 300 K, which is well above T_B. The magnetic moment is recorded during heating of the sample from 2 K to 300 K which is noted as the reference data. The sample is again cooled in zero field and is allowed to relax at a selective temperature where it is halted for several hours. In present case, the sample is cooled down from 300 K to 75 K (T_W) in zero field. After halting for 10000 s (2.77 hours) at 75 K, the cooling procedure is resumed to reach 2 K. Under applied field of 50 Oe, the magnetization M_{ZFC}^{halt} is recorded during subsequent heating. It is observed that the heating curve deviates from the reference ZFC (M_{ZFC}^{ref}) curve and the deviation is noticed well from ΔM ($=M_{ZFC}^{ref} - M_{ZFC}^{halt}$) Vs temperature plot shown in Fig. 5.2.6.

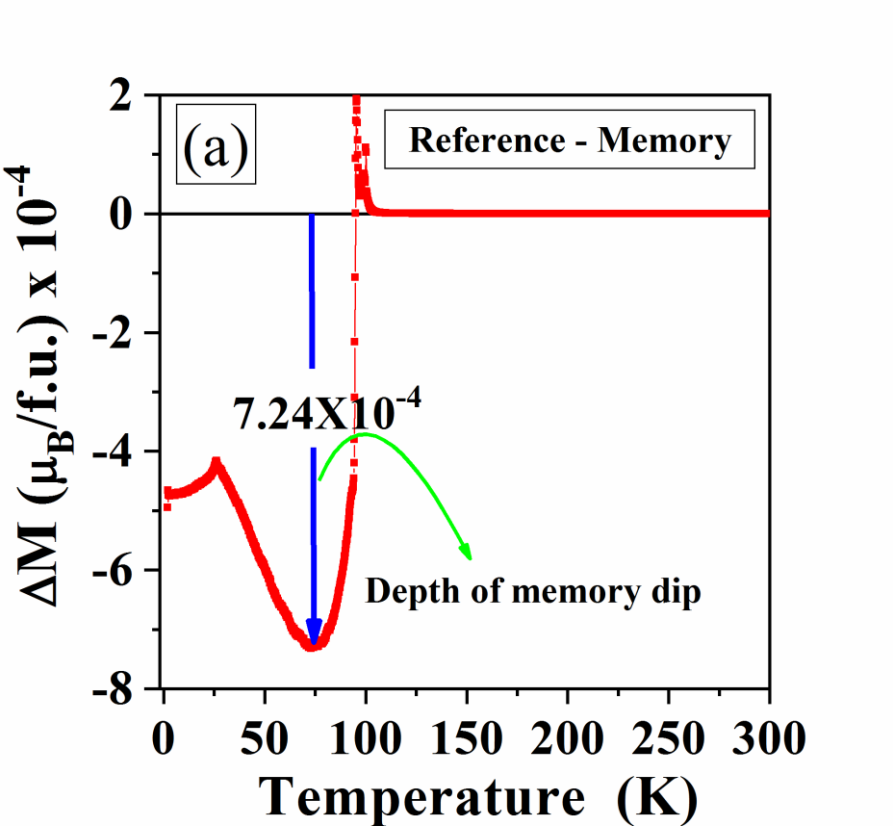

Fig. 5.2.6 The depth of memory effect observed at halt temperature 75K and halt time of 10000 s in ZFC protocol.

A prominent memory dip (ΔM) observed at 75 K in ZFC protocol is the signature of memory effect. The strength of memory effect can be interpreted in terms of the depth of the memory dip as shown in Fig. 5.2.6. The same procedure is repeated individually for different halt temperatures such as 30 K, 40 K, 50 K and 80 K having 10000 s (2.77 hours) halt at each temperature. The ΔM vs Temperature plot of corresponding halt temperature is summarized in Fig. 5.2.7. In general, the depth of memory dip varies with respect to halt temperature and halting time [Nadeem et al. (2015)].

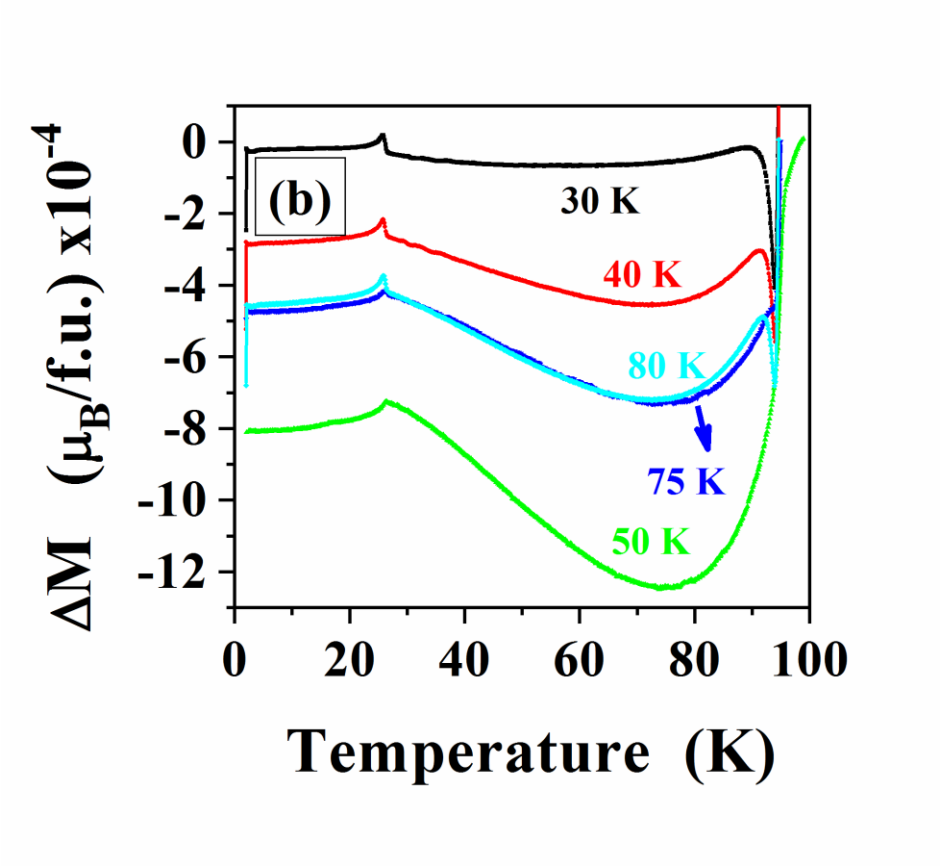

Fig. 5.2.7 The depth of memory effect observed for different halt temperatures. The ZFC memory effect experiment is performed at each temperature with a halt time of 10000 s.

For a constant halting time, a drop in magnetization is observed at every halt temperature as the magnetic moments equilibrate and depends on the magnetic state of the nanoparticles [Sayan et al. (2012)]. The depth of memory dip (ΔM) is high when the halt temperature is 50 K which decreases with decrease in halt temperature and vanishes at 30 K. Much below T_B, at 30 K, the drop in memory dip is less due to frozen shell spins. The amount of recovery in magnetization at every halt temperature depends on how fast the nanoparticles realign to the applied field. The most pronounced memory effect observed at 50 K, below T_B, could be due to the slow dynamics of the spin system. The less recovery of the spins could produce a large difference in reference and memory,

which shows a large memory dip at 50 K. Near to T_B, at 75 K the nanoparticles does not show the collective behavior. The de-blocking of the core spins and surface spins cause less drop in magnetization when the field is turned off for further cooling after halt time. Hence the depth of memory dip decreases at 75 K. Variation in exchange bias field (H_{EB}) and depth of memory dip with temperature is shown in Fig.5.2.8.

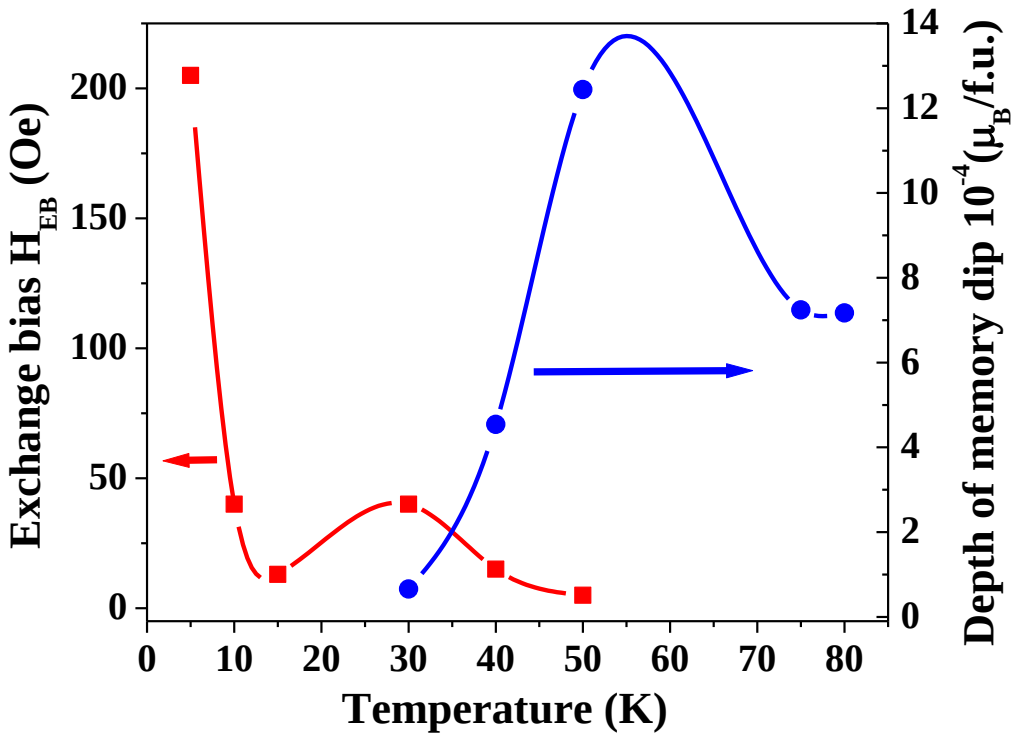

Fig. 5.2.8 Variation in exchange bias field (H_{EB}) and depth of memory dip with temperature.

While the depth of the memory effect decreases, the exchange bias increases with decrease in temperature. The observed decrease in depth of memory with increase in temperature is similar to the results observed in surfactant coated Fe_3O_4 nanoparticles studied by Suzuki *et al*. [Suzuki et al. (2009)] and in Ag doped with 11% of Mn studied

by Jonsson *et al* [Jonsson et al. (1999)]. Nadeem *et al.* have studied maghemite nanoparticles and reported that the position of memory dip observed at temperature where it is halted, which is generally observed in conventional spin glasses [Nadeem et al. (2015)]. In contrast, the position of memory dip observed in our case does not vary with the halt temperature. The appearance of memory dip at 75 K for all halt temperatures could be due to chaotic nature of the spin glass equilibrium configuration i.e., it is not a conventional spin glass. The unusual variation in memory effect could be attributed to broad particle size distribution leading to broad distribution in relaxation time [Biswas et al. (2014)]. The theoretical droplet and hierarchical models have been proposed to understand the nature of spin glass memory effect [Fisher et al. (1988); Vincent et al. (1995)]. This could be explained using hierarchical picture, which is generally used to explain the memory effect in nanoparticles. The hierarchical picture is characterized by a continuous splitting of the metastable states in phase space [Lefloch et al. (1992)]. The metastable states appear as local minima separated by finite barriers in the free-energy landscape. As the temperature increases, the metastable states continuously merge in to a single state called as global minima. The observed memory dip at 75 K, which does not change with halt temperature, could be due to merging of all metastable states into global minima.

5.3 Conclusions

$CoCr_2O_4$ nanoparticles having core shell structure shows a long range ferrimagnetic core surrounded by a shell with disordered spins. While the interaction between core and surface spins show exchange bias below spin-spiral transition (T_S), the memory effect is pronounced above T_S. Particularly, the EB effect decreases with increasing temperature

and nearly vanishes at 50 K. The depth of ΔM calculated from memory effect decreases with decreasing temperature and nearly vanishes at 30 K. In our case, the collapse of the memory dip occurs in the same temperature region in which EB starts developing. Unusually high exchange bias field obtained in $CoCr_2O_4$ nanoparticles was not only due to the contribution of interface between collinear and non-collinear spin alignment, rather due to spiral ordering below 30 K. We concluded that while the behavior of the training effect depends on the relative core to shell size ratio for a given nanoparticle size, the exchange bias is contributed by commensurate spiral ordering.